

The shifting of secondary inorganic aerosols formation mechanism during haze aggravation: The decisive role of aerosol liquid water

Fei Xie^{1,2}, Yue Su^{1,3}, Yongli Tian², Yanju Shi², Xingjun Zhou², Peng Wang², Ruihong Yu¹, Wei Wang¹, Jiang He^{1,3}, Jinyuan Xin^{4,*}, Changwei Lü^{1,3,*}

¹ School of Ecology and Environment, Inner Mongolia University, 010021, Hohhot, China

² Inner Mongolia Environmental Monitoring Center, 010011, Hohhot, China

³ Institute of Environmental Geology, Inner Mongolia University, 010021, Hohhot, China

⁴ State Key Laboratory of Atmospheric Boundary Layer Physics and Atmospheric Chemistry (LAPC), Institute of Atmospheric Physics, Chinese Academy of Sciences, Beijing 100029, China

Abstract

Although many considerable efforts have been done to reveal the driving factors on haze aggravation, however, the roles of aerosol liquid water (ALW) in SIAs formation were mainly focused on the condition of aerosol liquid water content (ALWC) $<100 \mu\text{g}/\text{m}^3$. Based on the in-situ high-resolution field observation, this work studied the decisive roles and the shifting of secondary inorganic aerosols formation mechanism during haze aggravation, revealing the different roles of ALWC in a broader scale ($\sim 500 \mu\text{g}/\text{m}^3$) in nitrate and sulfate formation induced by aqueous chemistry in ammonia-rich atmosphere. The results showed that chemical domains of perturbation gas limiting the generation of secondary particulate matters presented obvious shifts from HNO_3 sensitive to HNO_3 and NH_3 co-sensitive regime with the haze aggravation, indicating the powerful driving effects of ammonia in ammonia-rich atmosphere. When $\text{ALWC}<75 \mu\text{g}/\text{m}^3$, the sulfate generation was preferentially triggered by the high ammonia utilization, then accelerated by nitrogen oxide oxidation from Clean to Moderate pollution stages, characterizing as nitrogen oxidation ratio (NOR) <0.3 , sulfur oxidation ratio (SOR) <0.4 , ammonia transition ratio (NTR) <0.7 and the molar ratio of $\text{NO}_3^-/\text{SO}_4^{2-}=2:1$. While $\text{ALWC}>75 \mu\text{g}/\text{m}^3$, aqueous-phase chemistry reaction of SO_2 and NH_3 in ALW became the prerequisite for SIAs formation driven by Henry's law in the ammonia-rich atmosphere during Heavy and Serious stages, characterizing as high SOR (0.5-0.9), NOR (0.3-0.5), NTR (>0.7) and the molar ratio of $\text{NO}_3^-/\text{SO}_4^{2-}=1:1$. A positive feedback of sulfate on nitrate production was also observed in this work due to the shift of ammonia partition induced by the ALWC variation during haze aggravation. It implies the target controlling of haze should not simply focus on SO_2 and NO_2 , more attention should be paid on gaseous precursors (e.g., SO_2 , NO_2 , NH_3) and aerosol chemical constitution during different haze stages.

Keywords: Mechanism shifting, Aerosol liquid water, Secondary inorganic aerosols, Haze aggravation, In-situ observation

* Corresponding author, Email: xjy@mail.iap.ac.cn; lcw2008@imu.edu.cn

Deleted: u

Deleted: u

Deleted: u

Deleted: :

Deleted: u

Deleted: :

Deleted: .

Deleted: Our results provided the evidence that

Deleted: the transition ALWC affects sulfate and nitrate production by inducing a

Deleted: for the response of the transition ALWC with seasonal variability and climate change

47 **1 Introduction**

48 Fine particulate matter (PM_{2.5}) presented close link with several environmental issues, such as
49 visibility reduction and climate change (Zhang et al., 2015; Shang et al., 2020; Wang et al.,
50 2020; Wang et al., 2016; Nozière et al., 2010). Epidemiological studies have stated the
51 association of PMs with various public health, even adverse birth outcomes (Gwynn et al.,
52 2000; Lavigne et al., 2016; Zhao et al., 2020). As the most abundant secondary inorganic
53 aerosols (SIAs) in PM_{2.5} during Chinese winter haze episodes (Fu and Chen, 2017; Liu et al.,
54 2019), the formations of sulfate and nitrate play the key roles during haze aggravation, as well
55 as the impacting factors of the oxidants in gas and aqueous phases, the characteristics of pre-
56 existing aerosols/fog/cloud, and meteorological conditions. Recently, aerosol liquid water
57 content (ALWC) was reported associating with the SIAs formation, especially sulfates and
58 nitrates, during the haze periods (Wu et al., 2018; Zheng et al., 2015a; Wang et al., 2016; Cheng
59 et al., 2016; Carlton and Turpin, 2013; Nguyen et al., 2014; Xue et al., 2014; Tan et al., 2017;
60 Liu et al., 2017b). Atmospheric aerosol liquid water (ALW), which determined by ambient
61 relative humidity (RH), has been proposed as a container since it could provide the reaction
62 medium for the multiphase chemistry during the haze process (Ansari and Pandis, 2000;
63 Shiraiwa et al., 2012; Davies and Wilson, 2015). The roles of ALWC on the generations of
64 particulate sulfate generations (Wang et al., 2016; Cheng et al., 2016) and global secondary
65 organic aerosols (Hodas et al., 2014; McNeill, 2015; Wong et al., 2015) were reported. Thus,
66 fully understanding ALW and its roles during haze aggravation is fundamentally important on
67 atmospheric physicochemical processes, especially the liquid chemical transformation of SO₂
68 and NO_x in ALW.

69 Ammonia is the most important alkaline gas, neutralizing with acidic species to form
70 ammonium salts. Due to little attention has been paid to NH₃ emissions by Chinese government,
71 atmospheric NH₃ experienced a significant increasing trend (Ge et al., 2019; Tan et al., 2017).
72 Although the increase in atmospheric NH₃ is beneficial to reduce atmospheric acidity (Liu et
73 al., 2019), its chemical behavior on regional haze formation is still debating. Cheng et al. (2016)
74 indicated that the fast transform of gaseous SO₂ to particle sulfate under polluted conditions is
75 attributed to the neutralization of NH₃, which raises particle pH and thereby facilitated the
76 aqueous oxidation of S (VI) by NO₂. Fang et al. (2017) stated that NH₃ partition significantly
77 modified aerosol pH and thereby adjusting the partition of SO₂ and NO₂. Although the role of
78 NH₃ has been identified from a theoretical perspective, the lack of NH₃ emission control sets
79 barriers for more effective reduction of PM_{2.5}. Therefore, it is urgent to fully understand the
80 reactive gases behavior and the chemical mechanism of SIAs formation during different

- Deleted: , which formed by a mixture of both inorganic and organic species,
- Deleted: has important implications
- Deleted: for
- Formatted: Subscript
- Deleted: Synergistic adverse health effects have been observed between O₃ and aerosols, and e
- Deleted: shown that adverse health outcomes and even newborn healthcare associated with high concentrations of PMs
- Deleted: Due to the concentrated usage of coal, Chinese haze also featured as high loadings of sulfate, especially North China Plain (Wang et al., 2016). Meanwhile, high loadings of nitrate and ammonium, termed
- Deleted: as
- Deleted: , also featured as the most abundant species (>40%)
- Deleted: .
- Deleted: The production of sulfate and nitrate were highly depended on many factors, such as
- Deleted: levels of
- Deleted: both the
- Deleted: Accordingly, it is urgent to understand how they individually and collectively affect the production of SIA in different parts of the world.
- Deleted: Aerosol liquid water content (ALWC) was reported associating with the formation of secondary inorganic aerosols (SIAs), especially sulfates and nitrates, during the haze periods (Wu et al., 2018; Zheng et al., 2015a; Wang et al., 2016; Cheng et al., 2016; Carlton and Turpin, 2013; Nguyen et al., 2014; Xue et al., 2014; Tan et al., 2017; Liu et al., 2017b). Recently, t
- Deleted: Accordingly, despite the fact that enhanced emissions of NH₃(g) and other reactive gases may accelerate the neutralization of acidic particles and promoted SIA generation, the chemical regimes and behavior of reactive gases during different pollution are still debating and need to study in-depth....
- Deleted: regimes and behavior of reactive gases

118 pollution stages, which will be helpful to propose reasonable strategies for each stage.

Deleted: and

119 So far, the SIAs formation has been extensively studied during short-term, continuous, or
120 persistent haze episodes, proposing several heterogeneous and homogeneous oxidation
121 pathways on sulfate and nitrate formation (Guo et al., 2014; Guo et al., 2017; Zheng et al.,
122 2015b; Huang et al., 2014; Liu et al., 2021; Yao et al., 2020; Zhou et al., 2018; Liu et al., 2019).
123 In ammonia-rich atmosphere, NH₃ partition significantly modified aerosol pH, adjusted the
124 partition of SO₂ and NO₂ (Fang et al., 2017) and promotes the aqueous oxidation of S (VI) by
125 NO₂ (Wang et al., 2016; Cheng et al., 2016). Although many considerable efforts have been
126 done to reveal the driving factors on haze aggravation, however, the roles of ALW in SIAs
127 formation were mainly focused on the condition of ALWC<100 μg/m³ (Nenes et al., 2020; Wu
128 et al., 2018; Bian et al., 2014; Jin et al., 2020). Therefore, the roles of ALWC in a broader scale
129 and the mechanism shifting of secondary inorganic aerosols formation during haze aggravation
130 in ammonia-rich atmosphere need to be understood in depth. Based on a continuous
131 observation with 1-hour resolution from December 2019 to January 2020, this work discussed
132 the shift of dominant mechanism with ALWC variation during the time window of haze
133 aggravation processes, which will be helpful to propose more effective PM_{2.5} control strategies
134 for each pollution stage.

Deleted: of haze events

Deleted: will be helpful for fully understanding

Deleted: different

Deleted: levels

Deleted: different pollution stages and

Deleted: ing

Deleted:

Deleted: cities with significant characteristics of heating
seasonhaze aggravation processes

135 2 Sampling and Experiment Methods

136 2.1 Description of Sampling Site

137 Hohhot, the capital city of Inner Mongolia Autonomous Region, is the central city of Hohhot-
138 Baotou-Ordos group, as well as an important northern China city with a population of more
139 than 3.126 million and an area of 17224 km² (Fig. 1). This region is featured as continental
140 climate with marked seasonality changes, which characterized as long-lasting cold humid
141 winter and short-time other seasons. Thereby, to survive the cold season, approximately half
142 year of coal-fired heating events (Oct. 15-the following Apr. 15) were introduced, which
143 emitting gaseous pollutants as well as PMs around-the-clock. The main industries include
144 thermal power plants, coal-energy based biochemical industry, dairy industry and
145 petrochemical industry, etc., which also emit atmospheric pollutants ceaselessly. Thus, high
146 concentrations of PMs pollution cases dominated the major contamination cases during winter
147 season (data obtained from Department of Ecology and Environment of Inner Mongolia
148 Autonomous Region, <http://sthjt.nmg.gov.cn/>) and gradually emerging as the limiting factor on
149 regional ambient air quality and human health.

150 In this study, the observation was conducted at the Inner Mongolia Environmental
151

162 Monitoring Center (40°49'22"N, 111°45'2"E) on a top of a sixteen-story building (~40m above
 163 the ground level) located at the eastern part of the downtown near the People's Government of
 164 Inner Mongolia Autonomous Region near the 2nd ring road from December 1, 2019 to January
 165 31, 2020. Residential and administrative regions were characterized as the major functional
 166 domain near the sampling site, with no direct industrial regions nearby.

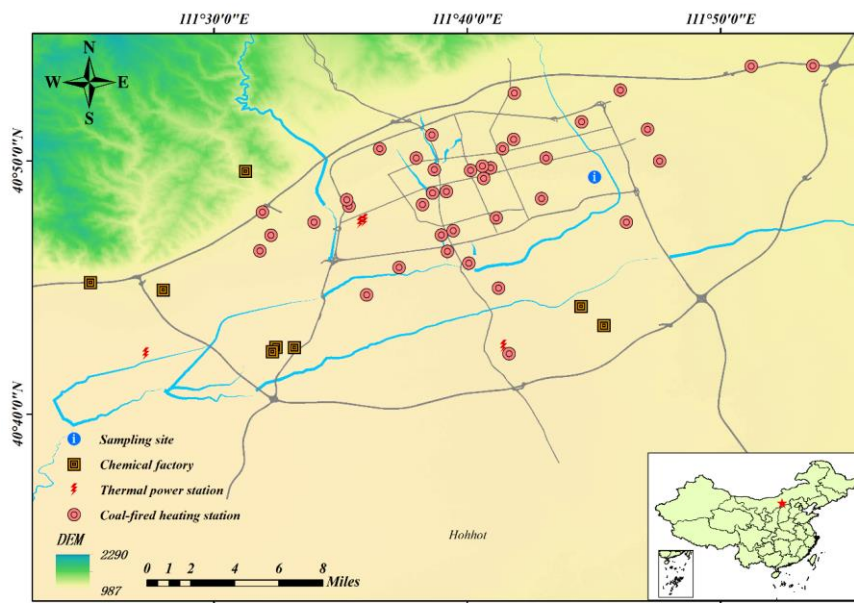


Fig. 1 Map of sampling sites and coal-fired enterprises

168
 169 **2.2 Data acquisition and analysis methods**

170 **2.2.1 Data acquisition**

171 On-line ion-chromatograph instrument (MARGA ADI 2080, Metrohm Applikon, Switzerland)
 172 was employed to simultaneously determine the water-soluble inorganic ions (Na^+ , NH_4^+ , Mg^{2+} ,
 173 Ca^{2+} , K^+ , Cl^- , F^- , SO_4^{2-} , NO_3^-) in $\text{PM}_{2.5}$ and corresponding trace gases (SO_2 , HNO_2 , HNO_3 , HCl ,
 174 NH_3). This instrument has been widely used in previous work (Rumsey et al., 2014; Nie et al.,
 175 2015; Huang et al., 2020) and the details were listed in Supplement (S1.1). Correspondingly,
 176 gaseous pollutants (e.g., NO_x , CO , PM_{10} , $\text{PM}_{2.5}$, PM_{10}) and meteorological datasets (e.g., wind
 177 speed, wind direction, RH, temperature, etc.), as well as the adopted models could be found in
 178 our previous work (Xie et al., 2021). In addition, peroxyacetyl nitrates (PANs), nitrous oxide
 179 (N_2O) and solar spectrophotometry were measured by PANs-100 (Focused Photonics Inc.),

Deleted:

Formatted: Heading 3, Line spacing: single

Deleted: acquire 9 particulate

Deleted: species

Deleted: as well as 5 categories of

Formatted: Subscript

Deleted:

Deleted: already

Deleted: precisely reported by

Deleted: numbers of

Deleted: elsewhere

Deleted: . In detail, 10 ppm H_2O_2 filled wet rotary denuder (WRD) were used to absorb the gaseous pollutants (e.g., HF, HCl, HNO_3 , HONO, SO_2 , NH_3), while particulate species (e.g., F, Cl, NO_3^- , SO_4^{2-} , NH_4^+ , Na^+ , K^+ , Mg^{2+} , Ca^{2+}) were collected by steam jet aerosol collector. By synchronizing occupying atmospheric sampling speed of 16.7L/min and WRD rotation speed of ≥ 8 rpm, the absorption efficiency of whole instrument reached greater than 99.7%, which makes the samples are reliable. Then, both gaseous and particulate samples are simultaneously transferred as liquid (aqueous) samples and analyzed by ion chromatography. An internal calibration standard containing Li^+ and Br^- with 1h-resolution was simultaneously injected with sample to account for any changes in the system. In addition, external standard solutions were also used to ensure peak identification and data quality. The detection limits of the particulate analytes were 0.001 $\mu\text{g}/\text{m}^3$, 0.005 $\mu\text{g}/\text{m}^3$, 0.004 $\mu\text{g}/\text{m}^3$, 0.005 $\mu\text{g}/\text{m}^3$, 0.005 $\mu\text{g}/\text{m}^3$, 0.009 $\mu\text{g}/\text{m}^3$, 0.006 $\mu\text{g}/\text{m}^3$, 0.009 $\mu\text{g}/\text{m}^3$ for Cl⁻, NO_3^- , SO_4^{2-} , NH_4^+ , Na^+ , K^+ , Mg^{2+} , Ca^{2+} , respectively. Gaseous analytes detection limits were 0.001 $\mu\text{g}/\text{m}^3$, 0.005 $\mu\text{g}/\text{m}^3$, 0.002 $\mu\text{g}/\text{m}^3$, 0.003 $\mu\text{g}/\text{m}^3$, 0.005 $\mu\text{g}/\text{m}^3$ for HCl, HNO_3 , HNO_2 , SO_2 , NH_3 , respectively.

Deleted: and gaseous pollutants (e.g., NO_x , CO , PM_{10} , $\text{PM}_{2.5}$, PM_{10}) ...

Deleted: equipment

Formatted: Subscript

214 N₂O Monitor (LSE, Monitors) and CE-318T (CIMEL), respectively.

216 2.2.2 Analysis methods

217 Generally, sulfur oxidation ratio (SOR) and nitrogen oxidation ratio (NOR) were calculated as
218 follows, which were used to indicate the contribution of secondary transformation during the
219 haze events (Song et al., 2007; Zhou et al., 2018).

$$SOR = \frac{n(SO_4^{2-})}{n(SO_2) + n(SO_4^{2-})}$$

$$NOR = \frac{n(HNO_3) + n(NO_3^-)}{n(NO_2) + n(HNO_3) + n(NO_3^-)}$$

222 Meanwhile, as an indicator of ammonia conversion efficient, ammonia transition ratio
223 (NTR), was calculated as the following equation (All units were $\mu\text{g}/\text{m}^3$).

$$NTR = \frac{NH_4^+/18}{NH_4^+/18 + NH_3/22.4}$$

225 In addition, as the fractions of ammonia, nitrate and sulfate in deliquesced aerosol, ϵ
226 (NO_3^-), $\epsilon(NH_4^+)$ and $\epsilon(SO_4^{2-})$ were expressed as follows.

$$\epsilon(NO_3^-) = \frac{n(NO_3^-)}{n(HNO_3) + n(NO_3^-)}$$

$$\epsilon(NH_4^+) = \frac{n(NH_4^+)}{n(NH_3) + n(NH_4^+)}$$

$$\epsilon(SO_4^{2-}) = \frac{n(SO_4^{2-})}{n(SO_2) + n(SO_4^{2-})}$$

230 2.2.3 Aerosol pH

231 In this work, a widely used thermodynamic model, ISORROPIA-II (Song et al., 2018; Gao et
232 al., 2020), was employed to establish aerosol acidity. Including the concentrations of WSIs in
233 PM_{2.5} and gaseous pollutions (e.g., NH₃, HCl), the simultaneously measured temperature and
234 RH data were imported into its Na⁺-K⁺-Ca²⁺-Mg²⁺-NH₄⁺-SO₄²⁻-NO₃⁻-Cl⁻-H₂O aerosol system.
235 According to previous study (Song et al., 2018) and our data profiles, “Forward Mode” and
236 “Metastable State” were selected in the model of ISORROPIA-II to calculate aerosol acidity
237 (H_{air}⁺, H⁺ loading per volume air ($\mu\text{g}/\text{m}^3$)) and aerosol liquid water content (ALWC). Then the
238 aerosol pH was calculated by the following equation.

$$pH = -\log_{10} \frac{1000H_{air}^+}{ALWC}$$

240 The concentrations of NH₃, NH₄⁺, NO₃⁻ and SO₄²⁻ modeled by this model significantly

Formatted: Heading 3, Line spacing: single

Deleted: SIA's formation processes always govern the aggravation of haze events. Thereby, to study the driven factors of SIA formation, ...ulfur oxidation ratio (SOR) and nitrogen oxidation ratio (NOR) were applied as indicators of oxidation rate in this work, which

Moved (insertion) [1]

Deleted: significant ...ontributions

Deleted: ,

Field Code Changed

Formatted: Line spacing: single

Moved up [1]: the significant contributions of secondary transformation during the haze events (Song et al., 2007; Zhou et al., 2018a).

Deleted: SOR and NOR were both higher than 0.1 in this work suggesting the significant contributions of secondary transformation during the haze events (Song et al., 2007; Zhou et al., 2018a). In addition

Formatted: Indent: First line: 0.74 cm

Deleted: also introduced in this work, which ...calculated as the following equation (All units were $\mu\text{g}/\text{m}^3$),

Formatted: Line spacing: single

Deleted: where all the units were presented in $\mu\text{g}/\text{m}^3$. Furthermore

Formatted: Indent: First line: 0.74 cm

Deleted: ,

Formatted: Line spacing: single

Deleted: Estimate a

Deleted: Methods to infer pH based on ion balances or ratios of measured anion and cations could not act as surrogates for pH due to OH⁻ or H⁺ could not taking into consideration(Guo et al., 2015; Guo et al., 2016). Thereby, to the best of our knowledge, the most accurate way to predict measure aerosol pH is to run a thermodynamic model on the basis of assuming the thermodynamic equilibrium. ...n this workHere...

ISORROPIA-II,...a widely used thermodynamic model,

Formatted

Deleted: using ...he following equation.,

Formatted: Line spacing: single

Deleted: where ALWC and H_{air}⁺ is the aerosol liquid water

344 [correlated with their measured values with correlation coefficients of 0.971-0.999, indicating](#)
345 [the accuracy and acceptability of the model in this work \(Fig. S1\).](#)

346 **2.2.4 Heterogeneous sulfate production**

347 Due to the necessity of precise SO_4^{2-} generation, heterogeneous sulfate production (P_{het}) was
348 parameterized and calculated according to the following equation (Jacob, 2000; Zheng et al.,
349 2015a).

$$P_{\text{het}} = \frac{3600sh^{-1} \times 96gmol^{-1} \times P}{R \times T} \left(\frac{R_p}{D_g} + \frac{4}{v\gamma} \right)^{-1} S_p[\text{SO}_2(g)]$$

351 Where P_{het} was presented in $\mu\text{g}\cdot\text{m}^{-3}\cdot\text{h}^{-1}$, 3600sh^{-1} is time conversion factor, 96 g/mol is the
352 molar mass of SO_4^{2-} , P is atmospheric pressure in kPa, R is the gas constant with the value of
353 $8.31\text{ Pa}\cdot\text{m}^3\cdot\text{mol}^{-1}\cdot\text{K}^{-1}$, T is the temperature with the unit of K, R_p represented the radius of
354 aerosol particles (m), D_g is the SO_2 molecular diffusion coefficient and v is the mean molecular
355 speed of SO_2 with the typical tropospheric value of $2 \times 10^{-5}\text{m}^2\cdot\text{s}^{-1}$ and $300\text{ m}\cdot\text{s}^{-1}$, respectively. γ
356 is the uptake coefficient of SO_2 on aerosols, S_p is the aerosol surface area per unit volume of
357 air ($\text{m}^2\cdot\text{m}^{-3}$) (Jacob, 2000). $\text{PM}_{2.5}$ mass concentrations ($\mu\text{g}\cdot\text{m}^{-3}$) and mean radius (m) during
358 campaign were roughly calculated utilizing the following empirical formula published by Guo
359 et al. (2014):

$$R_p = (0.254 \times C_{(\text{PM}_{2.5})} + 10.259) \times 10^{-9}$$

361 mean density of particles ρ was calculated and showed as $1.5 \times 10^6\text{ g}\cdot\text{m}^{-3}$ using the volume
362 and surface area formulas of a sphere (Guo et al., 2014). S_p was estimated from the following
363 formula:

$$S_p = \frac{C_{(\text{PM}_{2.5})} \times 10^{-6}\text{ g} \cdot \mu\text{g}^{-1}}{4/3 \cdot \pi R_p^3 \cdot \rho} \cdot 4\pi R_p^2$$

365 relative humidity-dependent γ were derived according to Zheng et al. (2015a) during the
366 campaign in this work and showed as the following formula:

$$\gamma = \begin{cases} 2 \times 10^{-5}, & \Psi \leq 50\%, \\ 2 \times 10^{-5} + \frac{5 \times 10^{-5} - 2 \times 10^{-5}}{100 - 50\%} \times (\Psi - 50\%), & 50\% \leq \Psi \leq 100\% \end{cases}$$

368 where Ψ referred to RH with the unit of %.

369 **3 Results and Discussion**

370 Based on National Ambient Air Quality Standards [of China](#) (HJ633-2012)
371 (https://www.mee.gov.cn/ywgz/fgbz/bz/bzwb/jcffbz/201203/t20120302_224166.shtml), air
372 quality index (AQI) was introduced in this work to classify pollution levels [\(Wang et al., 2015;](#)

Deleted: ,

Deleted: ranged

Deleted: from

Deleted: to

Deleted: and distributed around the 1:1 line

Deleted: which

Deleted: ed

Deleted: highly

Deleted: is

Formatted: Font: (Asian) 等线

Formatted: Heading 3, Line spacing: single

Deleted: The data acquisition and analysis methods were detailed in Supplementary Material (Supplement, S1.1.1-S1.1.2) and the estimating method of aerosol pH was provided in the section of S1.1.4. The heterogeneous sulfate production was estimated as follows:

Deleted: published by

Deleted: Jacob (2000) and Zheng et al. (2015a).

Deleted: , last access: Nov. 5, 2020

Field Code Changed

Deleted: (detailed in Supplement, S22)

391 [Kanchan et al., 2015; Xu et al., 2017](#)) and discuss the characteristics of atmospheric pollutants.
392 Briefly, daily concentrations of PM_{2.5} ranged from 0-75, 75-115, 115-150, 150-250 and >250
393 $\mu\text{g}/\text{m}^3$ were classified as clean (C), light polluted (L), moderate polluted (M), heavy polluted
394 (H) and serious polluted (S) periods, respectively.

395 **3.1 The observed evidence for ammonia-rich atmosphere**

396 The characteristics of atmospheric pollutants and meteorological parameters during the studied
397 period were summarized in Supplement (S2.1). In this work, molar ratios of NH_4^+ vs. anions
398 was used to identify the chemical species of ammonium salts (Zhou et al., 2018; Wang et al.,
399 2021; Liu et al., 2017b; Shi et al., 2019). The calculated results (Supplement, S2.2) showed the
400 predominant chemical species of ammonium gradually varied from the coexistence of
401 ammonium sulfate ($(\text{NH}_4)_2\text{SO}_4$) and ammonium nitrate (NH_4NO_3) to the coexistence of
402 $(\text{NH}_4)_2\text{SO}_4$, NH_4NO_3 and ammonium chloride (NH_4Cl) with haze aggravation (Fig. S5).
403 Further, the slope of fitted equation between excess- NH_4^+ and anions were still lower than 1:1
404 line after neutralized all the measured anions, indicating the ammonia-rich atmosphere (Fig.
405 S5c). To meet the national demand of ultra-low emissions activities (nearly two times lower
406 than former national standard) on gaseous pollutants, heavy usage of ammonia-containing
407 compounds in the process of desulfurization and denitrification (Solera García et al., 2017; Tan
408 et al., 2017) at broadly distributed thermal power plants (>300,000kWh) and the close-set coal-
409 fired heating stations (Fig. 1) resulted ammonia fugitive provided a reasonable explanation on
410 this ammonia-rich atmosphere. Although the retrofit of national demand of ultra-low emissions
411 activities on gaseous pollutants (nearly two times lower than former national standard) has
412 been completed, distributed coal-based enterprises could also emit substantial SO_2 and NO_2
413 and subjecting to heterogeneous reactions to further generate sulfate and nitrate and aggravated
414 the haze events (Fig. S7a, S7b).

415 To show the reaction between ammonia and nitric acid and the other formation processes
416 of nitrate in different (relative) concentrations of sulfate, the data of previous studies and
417 different pollution levels (C, L, M, H, S) in this work were plotted in Fig. 2. When
418 $[\text{NH}_4^+]/[\text{SO}_4^{2-}] \leq 1.5$, the nitrate formation associated with crustal elements rather than
419 ammonium; while $[\text{NH}_4^+]/[\text{SO}_4^{2-}] > 1.5$, the homogeneous gas-phase reactions between NH_3
420 and HNO_3 became the major pathway for atmospheric ammonia to form NH_4NO_3 (Pathak et
421 al., 2009; Liu et al., 2019). The results illustrated that the ammonia-rich regimes were not only
422 found in Hohhot, but also observed in Guangzhou (Huang et al., 2011), Chengdu (Huang et al.,
423 2018), Lanzhou USA West and East, India, Ireland, Europe, Qingdao, Italy, Lin'an (Pathak et
424 al., 2009) in recent decades (Fig. 2). It suggested that atmospheric oxidative modifications in

Deleted:

Deleted: S2

Deleted: 1

Deleted: S2

Deleted: 1

Formatted: Subscript

Formatted: Indent: First line: 0.74 cm

Deleted: ,

Deleted: The

Deleted: nitrate formation with $[\text{NH}_4^+]/[\text{SO}_4^{2-}] < 1.5$ was independent of ammonium

Deleted: ,

Deleted: \geq

Deleted: suggested

Formatted: Subscript

Deleted: had remarkable contributions on

Deleted: nitrate formation

Formatted: Subscript

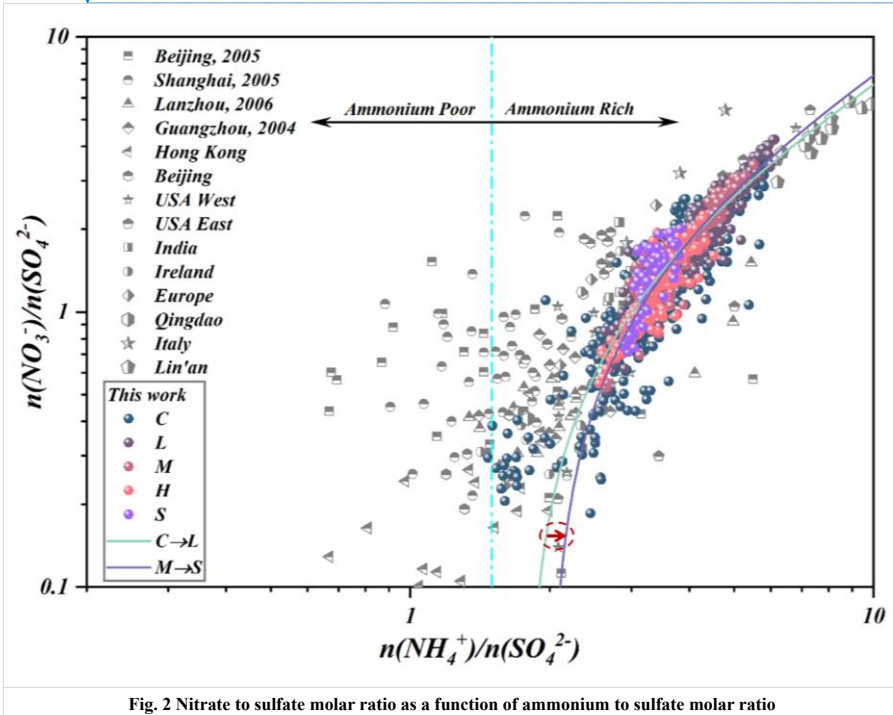
Formatted: Subscript

Formatted: Subscript

Deleted: . Thus, both most of scatters in previous works and our results indicating suggesting the characteristics of nitrate formed via the homogenous gas-phase reaction between ammonia and nitric acid

443 ammonia-rich atmosphere should be a widespread atmospheric issue with significant
 444 contributions on SIA generation. It was worth noting that the slopes of our data were becoming
 445 steeper, coupling with the $\text{NO}_3^-/\text{SO}_4^{2-}$ ratios change from ~ 4 to about 1, as the increasing
 446 pollution levels. The high $\text{PM}_{2.5}$ nitrate concentration during Heavy and Serious stages cannot
 447 be explained by the homogeneous gas-phase reaction involving ammonia and nitric acid, which
 448 may be associating with the heterogeneous reaction in ALW on the surface of the preexisting
 449 aerosols.

- Deleted: driven by excess ammonia
- Deleted: have been derived as
- Deleted: extremely
- Deleted: through multi-
- Deleted: .
- Deleted: reactions
- Deleted:



450
 451 **3.2 Driving mechanism of SIAs formation**

452 **3.2.1 Aerosol liquid water**

453 Our results showed that SOR, NOR, and SIAs in $\text{PM}_{2.5}$ presented increasing trends with the
 454 increasing ALWC during the five pollution levels. The variation of predominant chemical
 455 species of ammonium (Fig. 2) indicated more SIAs will be generated on particles with the
 456 simultaneous increase of ALWC and $\text{PM}_{2.5}$ (Fig.3b). Theoretically, the inorganic compounds
 457 conversion was enhanced via aqueous phase chemistry on moist particles owing to the
 458 continuous partition of gaseous pollutants (e.g., SO_2 , NO_2 , N_2O_5) in ALW, then disrupted the
 459 equilibrium between the gaseous and condensed phases, resulting in the aggravation of haze

Deleted: (the calculation detailed in Supplement, S1.1.3)

Deleted: C

469 events (Xue et al., 2014; Wu et al., 2018; Zheng et al., 2015b; Wang et al., 2016). Considering
470 seasonal heating characteristics, the shift of the equilibrium between gaseous and condensed
471 phases was enhanced with the increasing atmospheric pollutants concentrations due to the coal-
472 fired combustion events in winter. Detailly, owing to hygroscopic nature, the particles must
473 increase their water contents via ALW along with RH (Fig. S8a) to maintain thermodynamic
474 equilibrium and water vapor and simultaneously enhance the oxidation and dissolution of
475 precursors in the micro-solution (ALW) of the particulates. This process elevated the inorganic
476 mass fraction as well as particulate mass concentrations during different pollution stages (Fig.
477 S8b) (Bertram et al., 2009; Wang et al., 2016; Zheng et al., 2015a; Cheng et al., 2016). Due to
478 the larger affinity of H₂SO₄ for NH₃ (aq), sulfate was preferentially and fully neutralized by
479 ammonium in the ammonia-rich atmosphere to generate non-volatile nature of (NH₄)₂SO₄ (Liu
480 et al., 2017b; Zhou et al., 2018; Wang et al., 2021). Thus, SOR presented higher exponential
481 growth with the elevated AWLC coupling with more sulfate production (Fig. 3b).
482 Concomitantly, the preferentially generated (NH₄)₂SO₄ further enhanced the hygroscopicity of
483 particulate matter, in turn, helped more ammonia partitioning into moist particulate matter and
484 generating ammonium salts accelerating haze aggravation (Supplement, Fig. S6, Fig. S8c).
485 Thus, most important of all, the sharp increase of inorganic compounds associating with the
486 elevated ALWC significantly modified the specific surface area of particulates and further
487 accelerated the hygroscopic aerosol growth, which simultaneously provided a substrate for the
488 ensuing heterogenous reaction and accelerated the evolution of haze events. Previous work
489 reported that particles of different modes made different contributions to ALWC with the
490 contributions of nuclear, Aitken, accumulation and coarse modes assessed at <1%, 3%, 85%
491 and 12%, respectively, indicating that the contribution of accumulation mode particles to
492 ALWC dominated among all the aerosol particle modes (Tan et al., 2017). Meanwhile, the
493 observed significant correlations of ALWC with the ratios (PM_{1.0}/PM_{2.5} and PM_{2.5}/PM₁₀) in
494 this work also indicated that the hygroscopic growth of fine particulate matter (D_p ≤ 2.5 μm)
495 strongly associated with ALWC (Fig. 3a). Accordingly, both the previous work and our
496 monitoring results suggested that the ratios of PM_{1.0}/PM_{2.5} and PM_{2.5}/PM₁₀ could be used as
497 the proxy of the hygroscopic growth of particulate matter.

Deleted: in winter

Deleted: (Tan et al, 2017)

Deleted:

Deleted: (

Deleted:)

Deleted: This mechanism was confirmed that the proxy of hygroscopic growth of particulate matter (PM_{1.0}/PM_{2.5} and PM_{2.5}/PM₁₀) gradually increased with the increasing RH, even reaching at 95% (Fig. 3a).

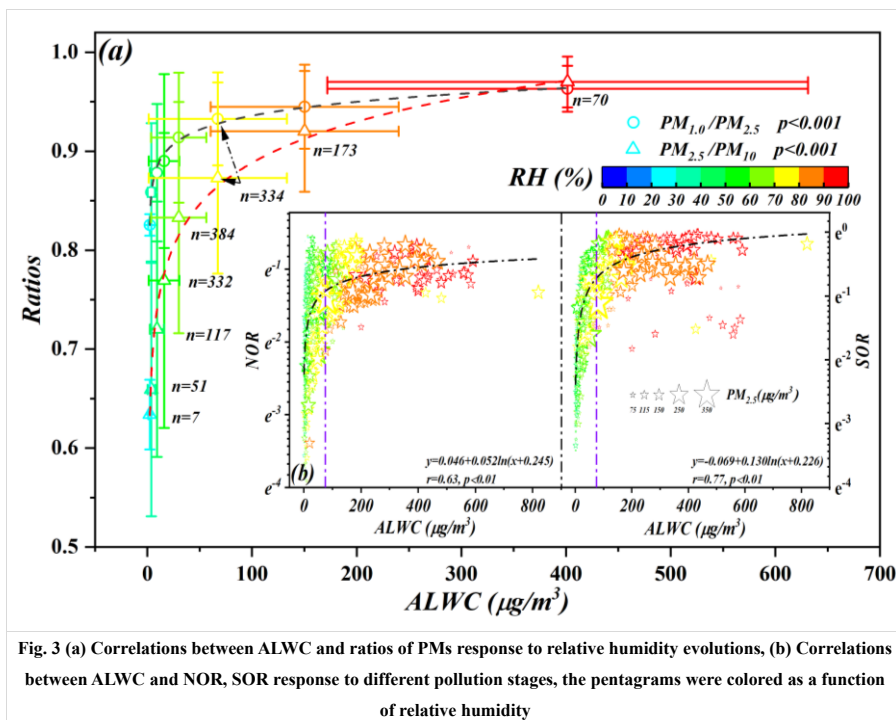


Fig. 3 (a) Correlations between ALWC and ratios of PMs response to relative humidity evolutions, (b) Correlations between ALWC and NOR, SOR response to different pollution stages, the pentagrams were colored as a function of relative humidity

508 3.2.2 Perturbation gases

509 Due to the strict control of SO_2 , atmospheric concentrations of NO_2 and NH_3 gradually became
 510 as the decisive reactive precursors on regional atmospheric secondary particulate matter
 511 generation. Thus, the state-of-the-art framework proposed by Nenes et al. (2020) was carried
 512 out to exam the chemical domain classifications and the decisive precursor based on the data
 513 sets of previous studies (Nenes et al., 2020) and this work (Fig. 4). Due to the
 514 thermodynamically stable property of the preferentially generated $(\text{NH}_4)_2\text{SO}_4$, the semi-
 515 volatile NH_4NO_3 dominate the partitioning of NH_3^{T} (sum of NH_3 and NH_4^+ , same to NO_3^{T})
 516 and NO_3^{T} . Although aqueous NO_3^- concentrations varied with haze processes, the calculated ϵ
 517 (NO_3^-) (detailed calculated method could be found in S1.2), which was an equilibrium
 518 parameter between gaseous HNO_3 and particle-phase NO_3^- (Guo et al., 2016; Fang et al., 2017),
 519 presented consistently full loadings of nitrate on the existing particulates during the studied
 520 period (Fig. S9a, Fig. S9b). This could provide clear evidence for the initial HNO_3 sensitive
 521 area and continuous control of HNO_3 during the studied periods. However, with haze
 522 aggravation, significant elevated ALWC resulted in more precursors partitioned in micro-
 523 droplets to maintain water vapor. This process induced a positive shift of HNO_3 dissolution

Deleted: a

Deleted: (ϵ (NOT 3))

Deleted: the results showed

Deleted: the

Deleted: Supplement, S1.2,

Deleted: (

Deleted:)

Deleted: (

Deleted:)

533 equilibrium and leading more HNO₃ partitioned on particles driven by the Henry's law (e.g.,
 534 HNO_{3(g)} ↔ HNO_{3(aq)}, $K_H = 2.07 \text{ mol}/(\text{L}\cdot\text{Pa})$). Meanwhile, HNO₃ and HONO could also produce
 535 through the reactions of $\text{NO}_2 + \text{H}_2\text{O} \xrightarrow{\text{Het}} \text{HNO}_3 + \text{HONO}$ (Huang et al., 2018). Accordingly,
 536 the OH radicals generated by HONO photolysis also contributed to this oxidation processes
 537 (Yue et al., 2020; Zhu et al., 2020). These aqueous oxidations processes were evidenced by the
 538 observation of significantly elevated HONO and PANs during the haze aggravation
 539 (Supplement, Fig. S7c, Fig. S7d). Accordingly, the equations of $\text{NH}_4^+ + \text{NO}_3^- + \text{H}^+ + \text{OH}^- \rightleftharpoons$
 540 $\text{NH}_4\text{NO}_3 + \text{H}_2\text{O}$ and $\text{NH}_4^+ + \text{SO}_4^{2-} + \text{H}^+ + \text{OH}^- \rightarrow (\text{NH}_4)_2\text{SO}_4 + \text{H}_2\text{O}$ were shifted to
 541 generate more NH₄NO₃ and (NH₄)₂SO₄ (Nenes et al., 2020; Xie et al., 2020) due to the driving
 542 force of more ammonia partitioned in elevated ALWC (NH₃+H₂O ⇌ NH₃·H₂O, NH₃·H₂O ⇌
 543 NH₄⁺+OH⁻). Therefore, NH₃ and NO_x became as the decisive factors on regional atmospheric
 544 oxidability in the ammonia-rich regime (Zhai et al., 2021; Tan et al., 2017; Liu et al., 2019; Li
 545 et al., 2019).

546 Generally, both NH₃ and HNO₃ were the limiting factors governing the aerosol generations
 547 for cities of North China due to high loadings of atmospheric ammonia, while NH₃ governed
 548 PM formation for the southeast US (SAS) (Zhao et al., 2020). Thanks to the raw data of
 549 Shenzhen (SZ) (Wang et al., 2022), we also calculated the ALWC and aerosol pH using
 550 ISORROPIA-II and the scatters of SZ suggested obvious chemical transition from HNO₃-NH₃
 551 regime to NH₃ sensitive regime due to the differently originated air masses. Although both
 552 cities located in US, the findings in California (CNX) were quite interesting and distributed in
 553 the insensitive region and the combined NH₃-HNO₃ sensitive region due to the moderate NH₃
 554 levels and the complicated atmospheric conditions during the observation (Nenes et al., 2020).
 555 In our work, the data points (541/744) in summer (pH=3.47 ± 1.29) mostly lied in HNO₃
 556 sensitive region, while chemical domains of perturbation gas limiting the generation of
 557 secondary particulate matters presented obvious shifts from HNO₃ sensitive to HNO₃ and NH₃
 558 co-sensitive regime with the haze aggravation in winter. Some data points of this work lied in
 559 the combined NH₃-HNO₃ region in winter owing to the more acidic condition. Under the stable
 560 pH of aerosols in winter at Hohhot (pH=4-5), the more important is that a fraction of points
 561 will distribute in the combined NH₃-HNO₃ region when ALWC > 75 μg/m³, which may be
 562 attributed to the aqueous chemical transformation driven by Henry's law mentioned above due
 563 to the elevating ALWC. Comparatively, the aerosols pH in summer was significantly lower
 564 than those in winter in Hohhot. Compared to TJ and SZ, the aerosols pH of Hohhot in winter
 565 was also significantly higher (Fig. 4) due to the acidity of atmospheric PM is largely depended
 566 on the alkaline material in surface soils in arid and semi-arid region and the elevated

Deleted: produced

Formatted: Not Highlight

Formatted: Subscript

Deleted: Then, the protons generated from acid dissociation in ALW activated the aqueous oxidation of the precursors to form stable acidic anions (e.g., SO₄²⁻, NO₃⁻) as well as other oxidizing agents (e.g., HONO,

Deleted: Meanwhile

Formatted: Not Highlight

Deleted: soluble transition metal ions, as well as

Deleted: ,

Deleted: Besides, the scatters in Shenzhen (SZ) also presented as significantly obvious chemical transition from HNO₃-NH₃ regime to NH₃ sensitive regime due to the notable different originated air masses

Deleted: .

Deleted: In winter,

Deleted: secondary inorganic

Deleted: μ

Deleted: liquid

Deleted: of

Deleted: secondary inorganic

Deleted: aerosols

Deleted: Tianjin

Deleted: secondary inorganic aerosols in

Formatted: Not Highlight

Deleted: both

Deleted: of China

Formatted: Not Highlight

Formatted: Not Highlight

591 atmospheric ammonia. In terms of seasonal characteristics, the higher temperature in summer
 592 elevates the volatility of NH_4NO_3 and dominates the partitioning of NH_3^{T} in atmospheric phase
 593 to decrease the pH of aerosols. Therefore, as can be seen from Fig. 4, the data points measured
 594 in winter Hohhot characterized as higher pH and low ALWC than those in summer (Hohhot,
 595 SAS, CNX, SZ). According to the framework of Nenes et al. (2020), the transition points of
 596 Hohhot (whether winter or summer) between NH_3 -dominated and HNO_3 -dominated sensitivity
 597 also occurs at a pH around 2 but at lower levels of ALWC. Theoretically, it should be associated
 598 with the more aridity of Hohhot locating in the arid and semi-arid region of China. Our results
 599 provided the evidence for “the additional insight” proposed by Nenes et al. (2020) that the
 600 transition ALWC varies with season change and the aridity of sites, in response to seasonal
 601 variability and climate change. Although this effort could provide sound explanation for
 602 limiting gaseous pollutants on PM formation, mechanisms on their chemical domains,
 603 especially the roles of ALW in different locations with various conditions need further study in
 604 the future.

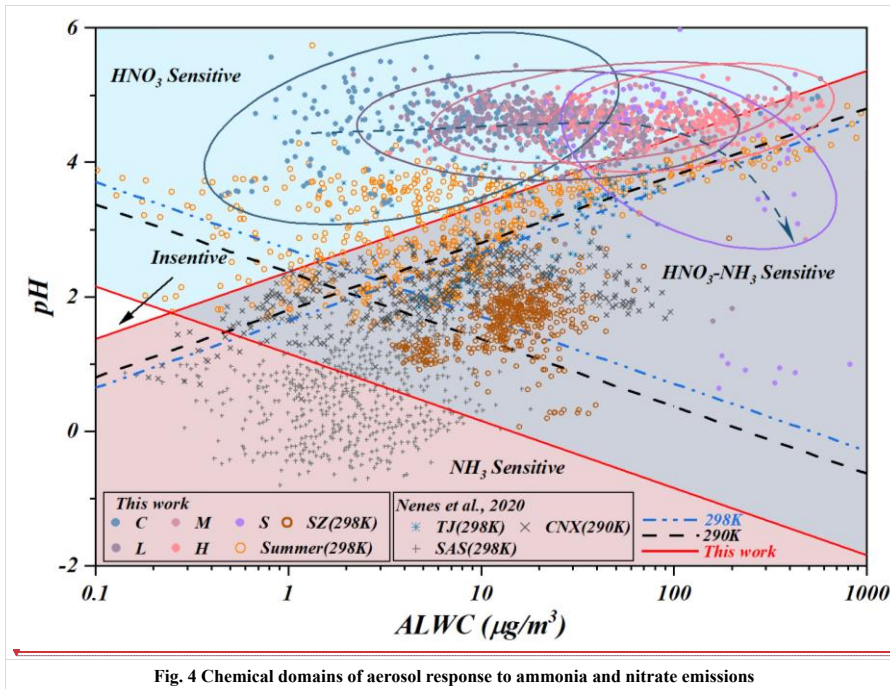


Fig. 4 Chemical domains of aerosol response to ammonia and nitrate emissions

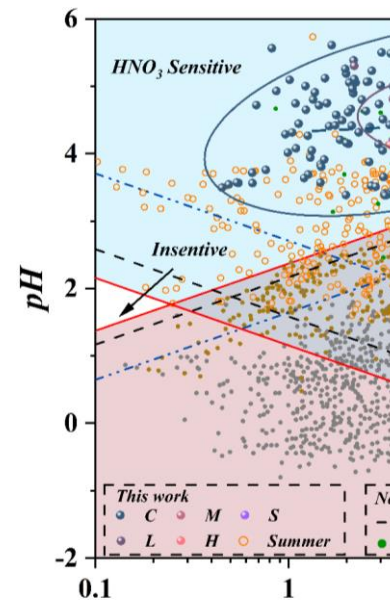
605 3.2.3 The shifting of SIAs formation mechanism driven by ALW

606 It's worth noting that two independent correlations were found between SOR and odd oxygen
 607 (O_x , $\text{O}_x = \text{NO}_2 + \text{O}_3$) during the aggravating processes of haze events, indicating the differential

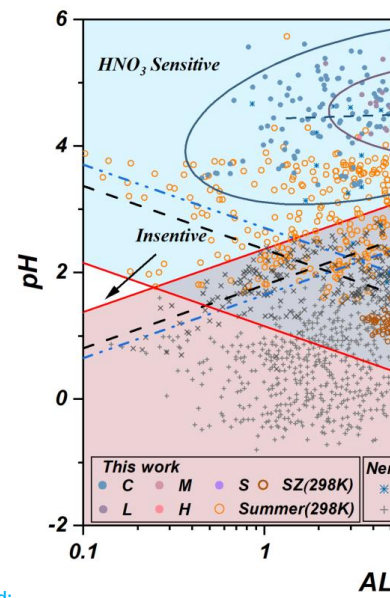
Deleted: um.... IThis was due to i

Deleted: I... terms of seasonal characteristics, the higher temperature in summer elevates the volatility of NH_4NO_3 and dominates the partitioning of NH_3^{T} in atmospheric phase to decrease the pH of secondary inorganic

Deleted: (...ohhot and Tianjin)

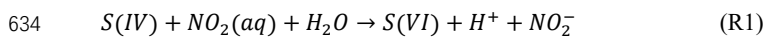


Deleted:

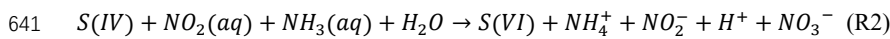


Deleted:

627 mechanisms of atmospheric oxidability on sulfate generations at different stages (Fig. 5a).
 628 Different to inefficient homogeneous sulfate oxidation efficiency (Supplement, Fig. S10),
 629 significant correlations pairs of NO₂ with SOR (Fig.5b) and NOR with SO₄²⁻ (Fig.5c) suggested
 630 the haze aggravation was largely related to the regional NO₂ levels due to the regulating effects
 631 on atmospheric oxidizability. Thus, the aqueous-phase oxidation of S(IV) by NO₂ (aq) was
 632 triggered and accelerated by the increasing ALWC and the following equation (Yao et al., 2020;
 633 Wang et al., 2016) (Supplement, Fig. S11a):



635 Meanwhile, sharp logarithmic increase between SOR and NH₄⁺ were also observed from Clean
 636 to Moderate pollution stages (Supplement, Fig. S12). Due to the joint effects of ammonia-rich
 637 atmosphere and ammonia's extremely water-soluble property, sufficient hydroxide generated
 638 by ammonia dissolution forced the NO₂ partitioned in ALW to maintain pH through
 639 neutralization and producing sulfate via R1. Thus, the following equation (R2) was derived
 640 with considering the processes of ammonia hydrolysis, which was evidenced by Fig. S11b.



642 Generally, NOR<0.1 means insignificant nitrogen oxide oxidation, therefore the observed
 643 regime shift of nitrate and ammonia chemical behavior on sulfate generation suggested the
 644 sulfate generation was preferentially triggered by the high ammonia utilization, then
 645 accelerated by the co-effects of ammonia utilization and nitrogen oxide oxidation (Fig. 5c).

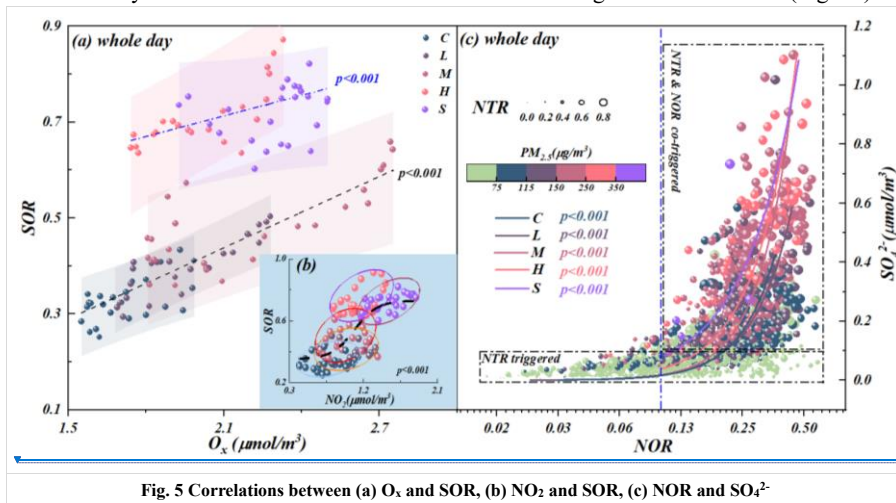
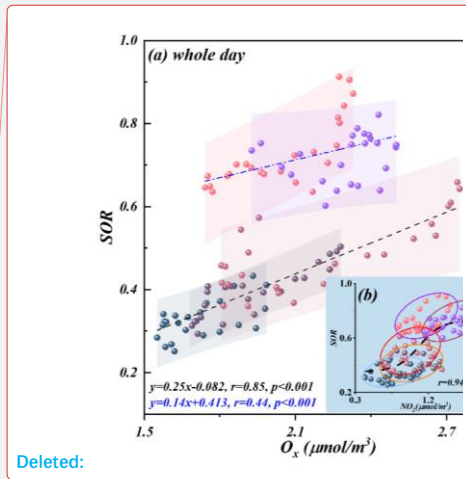
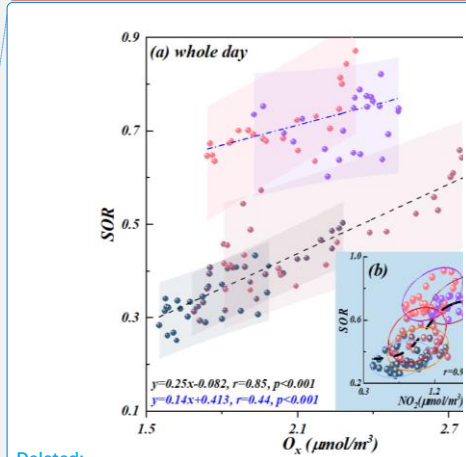


Fig. 5 Correlations between (a) O_x and SOR, (b) NO₂ and SOR, (c) NOR and SO₄²⁻

646 Accordingly, the reaction R2 was activated due to the increased ALWC forced more
 647 ammonia to partition into moist particulate matter driven by the Henry's law in the ammonia-
 648 rich atmosphere (NH_{3(g)}→NH_{3(aq)}) (Supplement, Fig. S9c) (Clegg et al., 1998; Wu et al., 2018;



Deleted:



Deleted:

Deleted: (

Deleted:)

653 Xie et al., 2020). Meanwhile, our calculated aqueous generated NO_3^- nicely matched theoretical
654 nitrate aqueous generation curve (the solid blue line in Fig. S9b) proposed by Guo et al. (2017),
655 suggesting the pathway of fast sulfate formation from oxidation of S(IV) by NO_2 to generate
656 HONO (Wang et al., 2020) (Supplement, Fig. S11) via the reaction R2. As a result, the
657 thermodynamically stable $(\text{NH}_4)_2\text{SO}_4$ would be preferentially formed to maintain its water
658 vapor pressure and thermodynamic equilibrium, then triggered the haze formation. Thus, the
659 mentioned effects resulted in a pronounced increase of NH_3 partitioning with the haze
660 aggravation, suggesting the importance of ammonia partition on sulfate generations, namely,
661 NTR-controlled regime with $\text{ALWC} < 75 \mu\text{g}/\text{m}^3$. In summary, when $\text{ALWC} < 75 \mu\text{g}/\text{m}^3$, the
662 sulfate generation was preferentially triggered by high ammonia utilization, then accelerated
663 by nitrogen oxide oxidation from Clean to Light pollution stages (Fig. 5c) with $\text{NOR} < 0.3$,
664 $\text{SOR} < 0.4$ and $\text{NTR} < 0.7$. In this period, the chemical composition of SIAs characterized as the
665 molar ratio of $\text{NO}_3^-:\text{SO}_4^{2-}=2:1$ (Fig. 6).

666 When $\text{ALWC} > 75 \mu\text{g}/\text{m}^3$, the haze was aggravated from Moderate to Serious stages along
667 with the increasing ALWC. As a result of increase in ALW, large amount of H^+ was dissociated
668 during the generation of ammonium sulfate (Supplement, Fig. S13a). From Light to Moderate
669 pollution stages, the solubility SO_2 driven by Henry's law was self-limiting due to the acidity
670 effect in low ALWC (with $\text{ALWC} < 75 \mu\text{g}/\text{m}^3$). Therefore, low sulfate concentrations coupled
671 with low ALWC at the beginning of haze event (Supplement, Fig. S13a). However, due to the
672 co-effects of elevated ALWC and hygroscopic nature of pre-generated ammonia sulfate, H^+
673 concentrations were diluted and nearly constant in-situ pH with the increase of ALWC during
674 Heavy and Serious pollution stages (Supplement, Fig. S14) (Wang et al., 2016; Clifton et al.,
675 1988; Huie and Neta, 1986; Lee and Schwartz, 1982). Hence, the significantly elevated ALWC
676 provided more chance for the partition of SO_2 , NO_2 and NH_3 in ALW from Moderate to Serious
677 pollution stages. Theoretically, Henry's constants of NO_2 ($9.74 \times 10^{-8} \text{ mol} \cdot (\text{L} \cdot \text{Pa})^{-1}$) is 3-4 orders
678 of magnitude lower than those of SO_2 ($1.22 \times 10^{-5} \text{ mol} \cdot (\text{L} \cdot \text{Pa})^{-1}$) and NH_3 (6.12×10^{-4}
679 $\text{ mol} \cdot (\text{L} \cdot \text{Pa})^{-1}$), however, it is worth noting that the aqueous generated NO_3^- from Moderate to
680 Serious stages rapidly increased 2-5 times higher than Clean and Light stages (Supplement,
681 Fig. S9b). Meanwhile, according to our monitoring results, the solar spectrophotometry at
682 380nm during Moderate to Serious stages was significantly lower than that in Clean stage,
683 (Supplement, Fig. S15), suggesting the aqueous oxidation of NO_2 was the predominant
684 compared to chain photolysis (Huang et al., 2018). Accordingly, it could be deduced that
685 aqueous-phase chemistry reaction of SO_2 and NH_3 in ALW, driven by Henry law, became the
686 dominant mechanism for sulfate formation due to more NO_2 was required to take part in the

Deleted: measured
Deleted: (
Deleted:)
Deleted: (Supplement, S1.2, Fig. S9(a), S9(b))

Deleted: S8b
Deleted: showed that
Deleted: from
Deleted: less
Deleted: 1/4 of
Deleted: c
Deleted: days
Deleted: at most
Deleted: predominant of NO_2
Deleted: than

701 fast sulfate formation with the increase of ALWC in the ammonia-rich atmosphere by the
 702 reaction R2. Thus, with the increasing of ALWC, high concentrations of sulfate and nitrate with
 703 high SOR (0.5-0.9), NOR (0.3-0.5) and NTR (>0.7) induced the haze events becoming Heavy
 704 and Serious levels (Fig. 5c). Simultaneously, the calculated heterogeneous sulfate production
 705 rate (Jacob, 2000; Meneill, 2015) (Supplement, Fig. S16) presented similar trends with the
 706 impacts of ammonia on sulfate production during different pollution stages (Xue et al., 2016;
 707 Cheng et al., 2016; Liu et al., 2020). It further stated the environmental significance of the
 708 partitioning of SO₂ and NH₃ between gas and aqueous (ALW) phases for SIAs formation and
 709 haze aggravation. Our results provided the evidence of significant negative correlations
 710 between HONO and N₂O (Supplement, Fig. S17) from Moderate to Serious stages and positive
 711 correlations between HONO and SOR (Supplement, Fig.S11a), highlighting the recent reported
 712 secondary aqueous-phase oxidation pathway of SO₂ by HONO from moderate pollution period
 713 ($2N(III) + 2S(IV) \rightarrow N_2O \uparrow + 2S(VI) + other\ products$) (Wang et al., 2020). In summary,
 714 when ALWC>75 μg/m³, aqueous-phase chemistry reaction of SO₂ and NH₃ in ALW became
 715 the prerequisite for SIAs formation driven by Henry's law in the ammonia-rich atmosphere
 716 during Heavy and Serious stages with high SOR (0.5-0.9), NOR (0.3-0.5), NTR (>0.7). In this
 717 period, the chemical composition of SIAs characterized as the molar ratio of NO₃⁻:SO₄²⁻=1:1
 718 (Fig. 6).

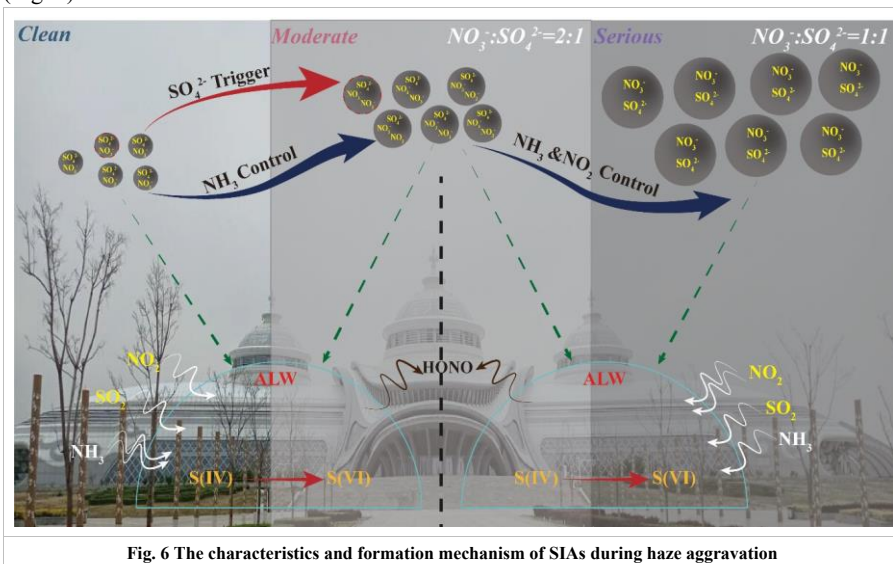


Fig. 6 The characteristics and formation mechanism of SIAs during haze aggravation

719

720 **3.2.4 The positive feedback of sulfate on nitrate production**

721 Previous works suggested that the homogeneous reaction of NO_2 with OH radicals during
722 daylight and heterogeneous hydrolysis of N_2O_5 at night were the main routes on nitrate
723 formation during haze episodes (He et al., 2018; Liu et al., 2020; Liu et al., 2019). Unsurprising,
724 higher nitrate production rates (ΔNO_3^- , the difference of hour concentrations and matrixing
725 afterwards) were frequently observed in ammonia-rich conditions due to that ammonia-rich
726 regime was more conducive on nitrate generation. However, the high level of nitrate production
727 rates (ΔNO_3^-) were found in the area characterizing as high ammonium and low sulfate levels,
728 suggesting that highly utilizing ammonium and pre-generated sulfate promoting particle-phase
729 nitrate generations (Fig. 7).

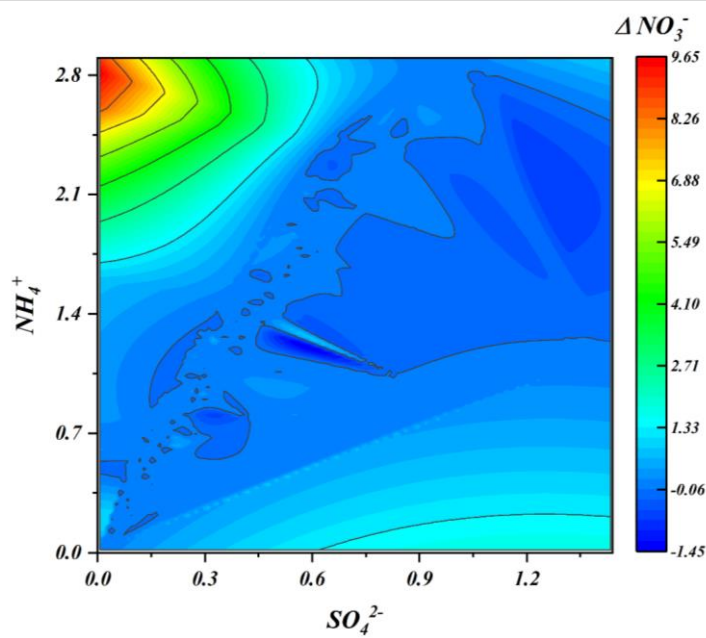
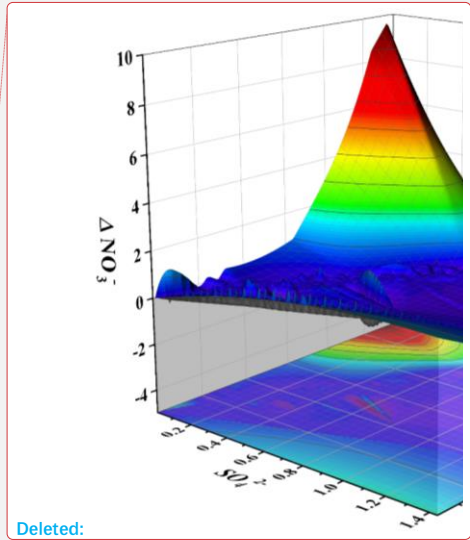


Fig. 7 Direct observation of nitrate production facilitated by initially generated sulfate.
(All data were matrixed to avoid interference caused by dimensionality)

730 Here, we proposed a hypothesis about the hydrogen ion concentration to respond the
731 above observations. As is known to all, apart from the extremely low levels of crustal elements,
732 ammonia is the only alkaline gas to neutralize the acidic gases in the atmosphere and generate
733 ammonium ions (Xie et al., 2020). Thus, the concentrations of particulate sulfate and nitrate
734 are affected by the partitioning of $\text{NH}_4^+/\text{NH}_3$. Thereby, higher values of ΔNO_3^- and ΔSO_4^{2-}
735



Deleted:

737 always occurred in the regions with higher ammonium ions were not confused (Fig. 7, Fig.
738 S18). According to both our results and published laboratory work (Wang et al., 2016), the
739 acidity of the particulate matter could be significantly modified by the bulk aqueous reaction
740 between NO₂ and SO₂, in which this reaction could be further enhanced due to in the presence
741 of NH₃. As a result of the increase in RH, the partitioning of atmospheric ammonia was broken
742 in a deep extent, which enhanced the neutralization of S(VI) by ammonia at the particle surface
743 to generate ammonium sulfate and dissociate huge H⁺ (Fig. S13b, red part). Simultaneously,
744 the ALWC did not raised significantly (Fig. S14b) at the beginning of haze event with relative
745 low sulfate concentrations. Thus, hydrogen ions generated from sulfate dissociation absorb
746 ammonia more effectively from the ammonia-rich atmosphere at low relative humidity during
747 the early pollution stages, which significantly promotes the net nitrate production. However,
748 due to the co-effects of elevated RH and hygroscopic nature of pre-generated ammonia sulfate,
749 H⁺ concentrations were diluted and shown as nearly constant in-situ pH (Fig. S14a). According
750 to previous works, the reaction between firstly generated sulfate and bisulfate with ammonia
751 were treated as the determination reaction on particle acidity (Weber et al., 2016; Liu et al.,
752 2017a). This reaction is self-limiting due to the acidity effect, namely that it increases the
753 acidity of aqueous phase and in turn reduces the efficiency of Henry's constant for SO₂
754 solubility and reaction rate and reduced the H⁺ formation rates from moderate periods,
755 compared with clean periods (Fig. S13b, blue) (Wang et al., 2016; Clifton et al., 1988; Huie
756 and Neta, 1986; Lee and Schwartz, 1982). Due to the co-effects of RH increase and
757 hygroscopic of sulfate, the ALWC was significantly elevated with the worsen of haze. Although
758 more H⁺ was generated in this process, no significant decrease in pH was found with the haze
759 aggravation due to the dilution effect of ALWC on H⁺. Previous works suggested that in the
760 case of ALWC increase, nitrate production is controlled by elevated H⁺ associating with the
761 increase of sulfate, namely, NO₃⁻ presented elevating trend with the increases of H⁺
762 concentration (Xie et al., 2020). Thus, although H⁺ from the dissociation of sulfuric acid and
763 full-loaded particle nitrate in conjunction with the haze aggravation generate particle HNO₃
764 (Fig. S19a) could forcing more ammonia partitioned on the particles to generate ammonium
765 nitrate (Fig. S19b), net nitrate production (ΔNO_3^-) was nearly consistent.

766 4 Conclusions

767 The formation of SIAs, especially sulfates and nitrates, was inherently associated with ALWC
768 during the haze aggravation, in which the roles of ALWC should be more significant in
769 ammonia-rich atmosphere. The novelty of our work is to find the shifting of secondary
770 inorganic aerosols formation mechanism during haze aggravation and explain the different

Deleted: at the beginning of haze event, termed as relative low sulfate concentrations,

Deleted: preferentially generated

Deleted: hydrolyzed

Deleted: during the early stages of contamination at low relative humidity

Deleted: could

Deleted: significantly

779 roles of ALWC in a broader scale ($\sim 500 \text{ ug/m}^3$) in ammonia-rich atmosphere based on the in-
780 situ high-resolution on-line monitoring data sets. The results showed that chemical domains of
781 perturbation gas limiting the generation of secondary particulate matters presented obvious
782 shifts from HNO_3 sensitive to HNO_3 and NH_3 co-sensitive regime with the haze aggravation,
783 indicating the powerful driving effects of ammonia in ammonia-rich atmosphere. When
784 $\text{ALWC} < 75 \text{ ug/m}^3$, the sulfate generation was preferentially triggered by the high ammonia
785 utilization, then accelerated by nitrogen oxide oxidation from Clean to Moderate pollution
786 stages, characterizing as $\text{NOR} < 0.3$, $\text{SOR} < 0.4$, $\text{NTR} < 0.7$ and the molar ratio of $\text{NO}_3^-:\text{SO}_4^{2-}=2:1$.
787 While $\text{ALWC} > 75 \text{ ug/m}^3$, aqueous-phase chemistry reaction of SO_2 and NH_3 in ALW became
788 the prerequisite for SIAs formation driven by Henry's law in the ammonia-rich atmosphere
789 during Heavy and Serious stages, characterizing as high SOR (0.5-0.9), NOR (0.3-0.5), NTR
790 (> 0.7) and the molar ratio of $\text{NO}_3^-:\text{SO}_4^{2-}=1:1$. A positive feedback of sulfate on nitrate
791 production was also observed in this work. Our work provides a potential explanation for the
792 interactive mechanism and feedback between nitric aqueous chemistry and sulfate formation
793 in ammonia-rich atmosphere based on high-resolution field observation. It implies the target
794 controlling of haze should not simply focus on SO_2 and NO_2 , more attention should be paid on
795 gaseous precursors (e.g., SO_2 , NO_2 , NH_3) and aerosol chemical constitution during different
796 haze stages.

797

798 *Data availability.* All data of this study are available from the corresponding author upon
799 reasonable request (lcw2008@imu.edu.cn).

800

801 *Supplement.* The Supplement related to this article is available online at

802

803 *Author Contributions.* FX: Data curation, Formal analysis, Software, Writing-original draft.
804 YS: Investigation, Formal analysis. YLT: Methodology, Software. YSH: Investigation, Formal
805 analysis. XJZ: Investigation, Formal analysis, Software. PW: Methodology, Investigation.
806 RHY: Software, Writing-review & editing. WW: Investigation, Validation, Writing-review &
807 editing. JH: Investigation, Methodology. JYX: Investigation, Validation, Supervision, Writing-
808 review & editing. CWL: Initiating and leading this research, Supervision, Writing-review &
809 editing.

810

811 *Competing interest.* The authors declared that they have no conflict of interest.

812

813 *Acknowledgments.* This work is supported by Science and Technology Major Project on Air
814 Pollution Prevention and Prediction in Hohhot-Baotou-Ordos Cities Group of Inner Mongolia
815 (No. 2020ZD0013), National Natural Science Foundation of China (No. 42167028, 41763014)
816 and Science Fund for Distinguished Young Scholars of Inner Mongolia (2019JQ05).

817

818 **References**

- 819 Ansari, A. S. and Pandis, S. N.: Water Absorption by Secondary Organic Aerosol and Its Effect on Inorganic
820 Aerosol Behavior, *Environ. Sci. Technol.*, 34, 71-77, 10.1021/es990717q, 2000.
- 821 Bertram, T. H., Thornton, J. A., Riedel, T. P., Middlebrook, A. M., Bahreini, R., Bates, T. S., Quinn, P. K., and
822 Coffman, D. J.: Direct observations of N₂O₅ reactivity on ambient aerosol particles, *Geophys. Res. Lett.*, 36,
823 <https://doi.org/10.1029/2009GL040248>, 2009.
- 824 Bian, Y. X., Zhao, C. S., Ma, N., Chen, J., and Xu, W. Y.: A study of aerosol liquid water content based on
825 hygroscopicity measurements at high relative humidity in the North China Plain Atmos. Chem. Phys., 14,
826 6417-6426, <https://doi.org/10.5194/acp-14-6417-2014>, 2014.
- 827 Carlton, A. and Turpin, B.: Particle partitioning potential of organic compounds is highest in the Eastern US and
828 driven by anthropogenic water, *Atmos. Chem. Phys.*, 13, 10203-10214, 2013.
- 829 Cheng, Y., Zheng, G., Wei, C., Mu, Q., Zheng, B., Wang, Z., Gao, M., Zhang, Q., He, K., Carmichael, G., Pöschl,
830 U., and Su, H.: Reactive nitrogen chemistry in aerosol water as a source of sulfate during haze events in
831 China, *Sci. Adv.*, 2, e1601530, 10.1126/sciadv.1601530, 2016.
- 832 Clegg, S. L., Brimblecombe, P., and Wexler, A. S.: Thermodynamic Model of the System H⁺-NH₄⁺-SO₄²⁻-NO₃⁻
833 -H₂O at Tropospheric Temperatures, *J. Phys. Chem. A*, 102, 2137-2154, 10.1021/jp973042r, 1998.
- 834 Clifton, C. L., Altstein, N., and Huie, R. E.: Rate constant for the reaction of nitrogen dioxide with sulfur(IV) over
835 the pH range 5.3-13, *Environ. Sci. Technol.*, 22, 586-589, 10.1021/es00170a018, 1988.
- 836 Davies, J. F. and Wilson, K. R.: Nanoscale interfacial gradients formed by the reactive uptake of OH radicals onto
837 viscous aerosol surfaces, *Chem. Sci.*, 6, 7020-7027, 10.1039/C5SC02326B, 2015.
- 838 Fang, T., Guo, H., Zeng, L., Verma, V., Nenes, A., and Weber, R. J.: Highly Acidic Ambient Particles, Soluble
839 Metals, and Oxidative Potential: A Link between Sulfate and Aerosol Toxicity, *Environ. Sci. Technol.*, 51,
840 2611-2620, 10.1021/acs.est.6b06151, 2017.
- 841 Fu, H. and Chen, J.: Formation, features and controlling strategies of severe haze-fog pollutions in China, *Sci.*
842 *Total Environ.*, 578, 121-138, <https://doi.org/10.1016/j.scitotenv.2016.10.201>, 2017.
- 843 Gao, J., Wei, Y., Shi, G., Yu, H., Zhang, Z., Song, S., Wang, W., Liang, D., and Feng, Y.: Roles of RH, aerosol pH
844 and sources in concentrations of secondary inorganic aerosols, during different pollution periods, *Atmos.*
845 *Environ.*, 241, 117770, <https://doi.org/10.1016/j.atmosenv.2020.117770>, 2020.
- 846 Ge, B., Xu, X., Ma, Z., Pan, X., Wang, Z., Lin, W., Ouyang, B., Xu, D., Lee, J., Zheng, M., Ji, D., Sun, Y., Dong,
847 H., Squires, F. A., Fu, P., and Wang, Z.: Role of Ammonia on the Feedback Between AWC and Inorganic
848 Aerosol Formation During Heavy Pollution in the North China Plain, *Earth Space Sci.*, 6, 1675-1693,
849 <https://doi.org/10.1029/2019EA000799>, 2019.
- 850 Guo, H., Liu, J., Froyd, K. D., Roberts, J. M., Veres, P. R., Hayes, P. L., Jimenez, J. L., Nenes, A., and Weber, R.
851 J.: Fine particle pH and gas-particle phase partitioning of inorganic species in Pasadena, California, during
852 the 2010 CalNex campaign, *Atmos. Chem. Phys.*, 17, 5703-5719, 10.5194/acp-17-5703-2017, 2017.
- 853 Guo, H., Sullivan, A. P., Campuzano-Jost, P., Schroder, J. C., Lopez-Hilfiker, F. D., Dibb, J. E., Jimenez, J. L.,
854 Thornton, J. A., Brown, S. S., Nenes, A., and Weber, R. J.: Fine particle pH and the partitioning of nitric

Formatted: Indent: Left: 0 cm, Hanging: 2.36 ch, First line:
-2.36 ch

Formatted: Indent: Left: 0 cm, Hanging: 2.36 ch, First line:
-2.36 ch

855 acid during winter in the northeastern United States, *J. Geophys. Res.: Atmos.*
856 , 121, 10,355-310,376, <https://doi.org/10.1002/2016JD025311>, 2016.

857 Guo, S., Hu, M., Zamora, M. L., Peng, J., Shang, D., Zheng, J., Du, Z., Wu, Z., Shao, M., Zeng, L., Molina, M.
858 J., and Zhang, R.: Elucidating severe urban haze formation in China, *Proc. Natl. Acad. Sci. USA*, 111,
859 17373-17378, 10.1073/pnas.1419604111, 2014.

860 Gwynn, R. C., Burnett, R. T., and Thurston, G. D.: A time-series analysis of acidic particulate matter and daily
861 mortality and morbidity in the Buffalo, New York, region, *Environ. Health Persp.*, 108, 125-133,
862 doi:10.1289/ehp.00108125, 2000.

863 He, P., Xie, Z., Chi, X., Yu, X., Fan, S., Kang, H., Liu, C., and Zhan, H.: Atmospheric $\Delta^{17}O(NO_3^-)$ reveals
864 nocturnal chemistry dominates nitrate production in Beijing haze, *Atmos. Chem. Phys.*, 18, 14465-14476,
865 10.5194/acp-18-14465-2018, 2018.

866 Hodas, N., Sullivan, A. P., Skog, K., Keutsch, F. N., Collett, J. L., Decesari, S., Facchini, M. C., Carlton, A. G.,
867 Laaksonen, A., and Turpin, B. J.: Aerosol Liquid Water Driven by Anthropogenic Nitrate: Implications for
868 Lifetimes of Water-Soluble Organic Gases and Potential for Secondary Organic Aerosol Formation, *Environ.*
869 *Sci. Technol.*, 48, 11127-11136, 10.1021/es5025096, 2014.

870 Huang, R.-J., Duan, J., Li, Y., Chen, Q., Chen, Y., Tang, M., Yang, L., Ni, H., Lin, C., Xu, W., Liu, Y., Chen, C.,
871 Yan, Z., Ovadnevaite, J., Ceburnis, D., Dusek, U., Cao, J., Hoffmann, T., and O'Dowd, C. D.: Effects of
872 NH_3 and alkaline metals on the formation of particulate sulfate and nitrate in wintertime Beijing, *Sci. Total*
873 *Environ.*, 717, 137190, <https://doi.org/10.1016/j.scitotenv.2020.137190>, 2020.

874 Huang, R.-J., Zhang, Y., Bozzetti, C., Ho, K.-F., Cao, J.-J., Han, Y., Daellenbach, K. R., Slowik, J. G., Platt, S. M.,
875 Canonaco, F., Zotter, P., Wolf, R., Pieber, S. M., Bruns, E. A., Crippa, M., Ciarelli, G., Piazzalunga, A.,
876 Schwikowski, M., Abbaszade, G., Schnelle-Kreis, J., Zimmermann, R., An, Z., Szidat, S., Baltensperger, U.,
877 Haddad, I. E., and Prévôt, A. S. H.: High secondary aerosol contribution to particulate pollution during haze
878 events in China, *Nature*, 514, 218-222, 10.1038/nature13774, 2014.

879 Huang, X., Qiu, R., Chan, C. K., and Ravi Kant, P.: Evidence of high $PM_{2.5}$ strong acidity in ammonia-rich
880 atmosphere of Guangzhou, China: Transition in pathways of ambient ammonia to form aerosol ammonium
881 at $[NH_4^+]/[SO_4^{2-}]=1.5$, *Atmos. Res.*, 99, 488-495, <https://doi.org/10.1016/j.atmosres.2010.11.021>, 2011.

882 Huang, X., Zhang, J., Luo, B., Wang, L., Tang, G., Liu, Z., Song, H., Zhang, W., Yuan, L., and Wang, Y.: Water-
883 soluble ions in $PM_{2.5}$ during spring haze and dust periods in Chengdu, China: Variations, nitrate formation
884 and potential source areas, *Environ. Pollut.*, 243, 1740-1749, <https://doi.org/10.1016/j.envpol.2018.09.126>,
885 2018.

886 Huie, R. E. and Neta, P.: Kinetics of one-electron transfer reactions involving chlorine dioxide and nitrogen
887 dioxide, *J. Phys. Chem.*, 90, 1193-1198, 10.1021/j100278a046, 1986.

888 Jacob, D. J.: Heterogeneous chemistry and tropospheric ozone, *Atmos. Environ.*, 34, 2131-2159,
889 [https://doi.org/10.1016/S1352-2310\(99\)00462-8](https://doi.org/10.1016/S1352-2310(99)00462-8), 2000.

890 Jin, X., Wang, Y., Li, Z., Zhang, F., Xu, W., Sun, Y., Fan, X., Chen, G., Wu, H., Ren, J., Wang, Q., and Cribb, M.:
891 Significant contribution of organics to aerosol liquid water content in winter in Beijing, China, *Atmos. Chem.*
892 *Phys.*, 20, 901-914, <https://doi.org/10.5194/acp-20-901-2020>, 2020.

893 Kanchan, K., Gorai, A. K., and Goyal, P.: A review on air quality indexing system, *Asian J Atmos. Environ.*, 9,
894 101-113, 2015.

895 Lavigne, E., Yasseen, A. S., Stieb, D. M., Hystad, P., van Donkelaar, A., Martin, R. V., Brook, J. R., Crouse, D.
896 L., Burnett, R. T., Chen, H., Weichenthal, S., Johnson, M., Villeneuve, P. J., and Walker, M.: Ambient air
897 pollution and adverse birth outcomes: Differences by maternal comorbidities, *Environ. Res.*, 148, 457-466,
898 <https://doi.org/10.1016/j.envres.2016.04.026>, 2016.

- 899 Lee, Y. and Schwartz, S.: Kinetics of oxidation of aqueous sulfur (IV) by nitrogen dioxide, Elsevier, New York,
900 pp 453-466 pp.1982.
- 901 Li, H., Cheng, J., Zhang, Q., Zheng, B., Zhang, Y., Zheng, G., and He, K.: Rapid transition in winter aerosol
902 composition in Beijing from 2014 to 2017: response to clean air actions, *Atmos. Chem. Phys.*, 19, 11485-
903 11499, 10.5194/acp-19-11485-2019, 2019.
- 904 Liu, M., Song, Y., Zhou, T., Xu, Z., Yan, C., Zheng, M., Wu, Z., Hu, M., Wu, Y., and Zhu, T.: Fine particle pH
905 during severe haze episodes in northern China, *Geophys. Res. Lett.*, 44, 5213-5221,
906 <https://doi.org/10.1002/2017GL073210>, 2017a.
- 907 Liu, M., Huang, X., Song, Y., Tang, J., Cao, J., Zhang, X., Zhang, Q., Wang, S., Xu, T., Kang, L., Cai, X., Zhang,
908 H., Yang, F., Wang, H., Yu, J. Z., Lau, A. K. H., He, L., Huang, X., Duan, L., Ding, A., Xue, L., Gao, J., Liu,
909 B., and Zhu, T.: Ammonia emission control in China would mitigate haze pollution and nitrogen deposition,
910 but worsen acid rain, *Proc. Natl. Acad. Sci. USA*, 116, 7760-7765, 10.1073/pnas.1814880116, 2019.
- 911 Liu, P., Ye, C., Xue, C., Zhang, C., Mu, Y., and Sun, X.: Formation mechanisms of atmospheric nitrate and sulfate
912 during the winter haze pollution periods in Beijing: gas-phase, heterogeneous and aqueous-phase chemistry,
913 *Atmos. Chem. Phys.*, 20, 4153-4165, 10.5194/acp-20-4153-2020, 2020.
- 914 Liu, T., Chan, A. W. H., and Abbatt, J. P. D.: Multiphase Oxidation of Sulfur Dioxide in Aerosol Particles:
915 Implications for Sulfate Formation in Polluted Environments, *Environ. Sci. Technol.*, 55, 4227-4242,
916 10.1021/acs.est.0c06496, 2021.
- 917 Liu, Z., Xie, Y., Hu, B., Wen, T., Xin, J., Li, X., and Wang, Y.: Size-resolved aerosol water-soluble ions during the
918 summer and winter seasons in Beijing: Formation mechanisms of secondary inorganic aerosols,
919 *Chemosphere*, 183, 119-131, <https://doi.org/10.1016/j.chemosphere.2017.05.095>, 2017b.
- 920 McNeill, V. F.: Aqueous Organic Chemistry in the Atmosphere: Sources and Chemical Processing of Organic
921 Aerosols, *Environ. Sci. Technol.*, 49, 1237-1244, 10.1021/es5043707, 2015.
- 922 Nenes, A., Pandis, S. N., Weber, R. J., and Russell, A.: Aerosol pH and liquid water content determine when
923 particulate matter is sensitive to ammonia and nitrate availability, *Atmos. Chem. Phys.*, 20, 3249-3258,
924 10.5194/acp-20-3249-2020, 2020.
- 925 Nguyen, T., Petters, M., Suda, S., Guo, H., Weber, R., and Carlton, A.: Trends in particle-phase liquid water during
926 the Southern Oxidant and Aerosol Study, *Atmos. Chem. Phys.*, 14, 10911-10930, 2014.
- 927 Nie, W., Ding, A. J., Xie, Y. N., Xu, Z., Mao, H., Kerminen, V. M., Zheng, L. F., Qi, X. M., Huang, X., Yang, X.
928 Q., Sun, J. N., Herrmann, E., Petäjä, T., Kulmala, M., and Fu, C. B.: Influence of biomass burning plumes
929 on HONO chemistry in eastern China, *Atmos. Chem. Phys.*, 15, 1147-1159, 10.5194/acp-15-1147-2015,
930 2015.
- 931 Nozière, B., Dziejic, P., and Córdoba, A.: Inorganic ammonium salts and carbonate salts are efficient catalysts
932 for aldol condensation in atmospheric aerosols, *Phys. Chem. Chem. Phys.*, 12, 3864-3872,
933 10.1039/B924443C, 2010.
- 934 Pathak, R. K., Wu, W. S., and Wang, T.: Summertime PM_{2.5} ionic species in four major cities of China: nitrate
935 formation in an ammonia-deficient atmosphere, *Atmos. Chem. Phys.*, 9, 1711-1722, 10.5194/acp-9-1711-
936 2009, 2009.
- 937 Rumsey, I. C., Cowen, K. A., Walker, J. T., Kelly, T. J., Hanft, E. A., Mishoe, K., Rogers, C., Proost, R., Beachley,
938 G. M., Lear, G., Frelink, T., and Otjes, R. P.: An assessment of the performance of the Monitor for Aerosols
939 and Gases in ambient air (MARGA): a semi-continuous method for soluble compounds, *Atmos. Chem.
940 Phys.*, 14, 5639-5658, 10.5194/acp-14-5639-2014, 2014.
- 941 Shang, D., Peng, J., Guo, S., Wu, Z., and Hu, M.: Secondary aerosol formation in winter haze over the Beijing-
942 Tianjin-Hebei Region, China, *Front Env. Sci. Eng.*, 15, 34, 10.1007/s11783-020-1326-x, 2020.

943 Shi, G., Xu, J., Shi, X., Liu, B., Bi, X., Xiao, Z., Chen, K., Wen, J., Dong, S., Tian, Y., Feng, Y., Yu, H., Song, S.,
944 Zhao, Q., Gao, J., and Russell, A. G.: Aerosol pH Dynamics During Haze Periods in an Urban Environment
945 in China: Use of Detailed, Hourly, Speciated Observations to Study the Role of Ammonia Availability and
946 Secondary Aerosol Formation and Urban Environment, *J. Geophys. Res.: Atmos.*
947 , 124, 9730-9742, <https://doi.org/10.1029/2018JD029976>, 2019.
948 Shiraiwa, M., Pfrang, C., Koop, T., and Pöschl, U.: Kinetic multi-layer model of gas-particle interactions in
949 aerosols and clouds (KM-GAP): linking condensation, evaporation and chemical reactions of organics,
950 oxidants and water, *Atmos. Chem. Phys.*, 12, 2777-2794, 10.5194/acp-12-2777-2012, 2012.
951 Solera García, M. A., Timmis, R. J., Van Dijk, N., Whyatt, J. D., Leith, I. D., Leeson, S. R., Braban, C. F., Sheppard,
952 L. J., Sutton, M. A., and Tang, Y. S.: Directional passive ambient air monitoring of ammonia for fugitive
953 source attribution; a field trial with wind tunnel characteristics, *Atmos. Environ.*, 167, 576-585,
954 <https://doi.org/10.1016/j.atmosenv.2017.07.043>, 2017.
955 Song, C. H., Kim, C. M., Lee, Y. J., Carmichael, G. R., Lee, B. K., and Lee, D. S.: An evaluation of reaction
956 probabilities of sulfate and nitrate precursors onto East Asian dust particles, *J. Geophys. Res. Atmos.*, 112,
957 D18206, <https://doi.org/10.1029/2006JD008092>, 2007.
958 Song, S., Gao, M., Xu, W., Shao, J., Shi, G., Wang, S., Wang, Y., Sun, Y., and McElroy, M. B.: Fine-particle pH
959 for Beijing winter haze as inferred from different thermodynamic equilibrium models, *Atmos. Chem. Phys.*,
960 18, 7423-7438, 10.5194/acp-18-7423-2018, 2018.
961 Tan, H., Cai, M., Fan, Q., Liu, L., Li, F., Chan, P., Deng, X., and Wu, D.: An analysis of aerosol liquid water
962 content and related impact factors in Pearl River Delta, *Sci. Total Environ.*, 579, 1822-1830, 2017.
963 Wang, G., Zhang, R., Gomez, M. E., Yang, L., Zamora, M. L., Hu, M., Lin, Y., Peng, J., Guo, S., and Meng, J.:
964 Persistent sulfate formation from London Fog to Chinese haze, *Proc. Natl. Acad. Sci. USA*, 113, 13630-
965 13635, 2016.
966 Wang, G., Chen, J., Xu, J., Yun, L., Zhang, M., Li, H., Qin, X., Deng, C., Zheng, H., Gui, H., Liu, J., and Huang,
967 K.: Atmospheric Processing at the Sea-Land Interface Over the South China Sea: Secondary Aerosol
968 Formation, Aerosol Acidity, and Role of Sea Salts, *J. Geophys. Res.: Atmos.*
969 , 127, e2021JD036255, <https://doi.org/10.1029/2021JD036255>, 2022.
970 Wang, H., Wang, X., Zhou, H., Ma, H., Xie, F., Zhou, X., Fan, Q., Lü, C., and He, J.: Stoichiometric characteristics
971 and economic implications of water-soluble ions in PM_{2.5} from a resource-dependent city, *Environ. Res.*,
972 193, 110522, <https://doi.org/10.1016/j.envres.2020.110522>, 2021.
973 Wang, J., Li, J., Ye, J., Zhao, J., and Jacob, D. J.: Fast sulfate formation from oxidation of SO₂ by NO₂ and HONO
974 observed in Beijing haze, *Nat. Commun.*, 11, 2844, 2020.
975 Wang, S., Nan, J., Shi, C., Fu, Q., Gao, S., Wang, D., Cui, H., Saiz-Lopez, A., and Zhou, B.: Atmospheric ammonia
976 and its impacts on regional air quality over the megacity of Shanghai, China, *Sci. Rep.*, 5, 15842,
977 10.1038/srep15842, 2015.
978 Weber, R. J., Guo, H., Russell, A. G., and Nenes, A.: High aerosol acidity despite declining atmospheric sulfate
979 concentrations over the past 15 years, *Nat. Geosci.*, 9, 282-285, 10.1038/ngeo2665, 2016.
980 Wong, J. P. S., Lee, A. K. Y., and Abbatt, J. P. D.: Impacts of Sulfate Seed Acidity and Water Content on Isoprene
981 Secondary Organic Aerosol Formation, *Environ. Sci. Technol.*, 49, 13215-13221, 10.1021/acs.est.5b02686,
982 2015.
983 Wu, Z., Wang, Y., Tan, T., Zhu, Y., Li, M., Shang, D., Wang, H., Lu, K., Guo, S., Zeng, L., and Zhang, Y.: Aerosol
984 Liquid Water Driven by Anthropogenic Inorganic Salts: Implying Its Key Role in Haze Formation over the
985 North China Plain, *Environ. Sci. Technol. Lett.*, 5, 160-166, 10.1021/acs.estlett.8b00021, 2018.
986 Xie, F., Zhou, X., Wang, H., Gao, J., Hao, F., He, J., and Lü, C.: Heating events drive the seasonal patterns of

987 volatile organic compounds in a typical semi-arid city, *Sci. Total Environ.*, 788, 147781,
988 <https://doi.org/10.1016/j.scitotenv.2021.147781>, 2021.

989 Xie, Y., Wang, G., Wang, X., Chen, J., Chen, Y., Tang, G., Wang, L., Ge, S., Xue, G., Wang, Y., and Gao, J.:
990 Nitrate-dominated PM_{2.5} and elevation of particle pH observed in urban Beijing during the winter of 2017,
991 *Atmos. Chem. Phys.*, 20, 5019-5033, 10.5194/acp-20-5019-2020, 2020.

992 Xu, L., Duan, F., He, K., Ma, Y., Zhu, L., Zheng, Y., Huang, T., Kimoto, T., Ma, T., Li, H., Ye, S., Yang, S., Sun,
993 Z., and Xu, B.: Characteristics of the secondary water-soluble ions in a typical autumn haze in Beijing,
994 *Environ. Pollut.*, 227, 296-305, <https://doi.org/10.1016/j.envpol.2017.04.076>, 2017.

995 Xue, J., Griffith, S. M., Yu, X., Lau, A. K. H., and Yu, J. Z.: Effect of nitrate and sulfate relative abundance in
996 PM_{2.5} on liquid water content explored through half-hourly observations of inorganic soluble aerosols at a
997 polluted receptor site, *Atmos. Environ.*, 99, 24-31, <https://doi.org/10.1016/j.atmosenv.2014.09.049>, 2014.

998 Xue, J., Yuan, Z., Griffith, S. M., Yu, X., Lau, A. K. H., and Yu, J. Z.: Sulfate Formation Enhanced by a Cocktail
999 of High NO_x, SO₂, Particulate Matter, and Droplet pH during Haze-Fog Events in Megacities in China: An
1000 Observation-Based Modeling Investigation, *Environ. Sci. Technol.*, 50, 7325-7334,
1001 10.1021/acs.est.6b00768, 2016.

1002 Yao, L., Fan, X., Yan, C., Kurtén, T., Daellenbach, K. R., Li, C., Wang, Y., Guo, Y., Dada, L., Rissanen, M. P., Cai,
1003 J., Tham, Y. J., Zha, Q., Zhang, S., Du, W., Yu, M., Zheng, F., Zhou, Y., Kontkanen, J., Chan, T., Shen, J.,
1004 Kujansuu, J. T., Kangasluoma, J., Jiang, J., Wang, L., Worsnop, D. R., Petäjä, T., Kerminen, V.-M., Liu, Y.,
1005 Chu, B., He, H., Kulmala, M., and Bianchi, F.: Unprecedented Ambient Sulfur Trioxide (SO₃) Detection:
1006 Possible Formation Mechanism and Atmospheric Implications, *Environ. Sci. Technol. Lett.*, 7, 809-818,
1007 10.1021/acs.estlett.0c00615, 2020.

1008 Yue, F., He, P., Chi, X., Wang, L., Yu, X., Zhang, P., and Xie, Z.: Characteristics and major influencing factors of
1009 sulfate production via heterogeneous transition-metal-catalyzed oxidation during haze evolution in China,
1010 *Atmos. Pollut. Res.*, 11, 1351-1358, <https://doi.org/10.1016/j.apr.2020.05.014>, 2020.

1011 Zhai, S., Jacob, D. J., Wang, X., Liu, Z., Wen, T., Shah, V., Li, K., Moch, J. M., Bates, K. H., Song, S., Shen, L.,
1012 Zhang, Y., Luo, G., Yu, F., Sun, Y., Wang, L., Qi, M., Tao, J., Gui, K., Xu, H., Zhang, Q., Zhao, T., Wang,
1013 Y., Lee, H. C., Choi, H., and Liao, H.: Control of particulate nitrate air pollution in China, *Nat. Geosci.*,
1014 10.1038/s41561-021-00726-z, 2021.

1015 Zhang, R., Wang, G., Guo, S., Zamora, M. L., Ying, Q., Lin, Y., Wang, W., Hu, M., and Wang, Y.: Formation of
1016 Urban Fine Particulate Matter, *Chem. Rev.*, 115, 3803-3855, 10.1021/acs.chemrev.5b00067, 2015.

1017 Zhao, Q., Nenes, A., Yu, H., Song, S., Xiao, Z., Chen, K., Shi, G., Feng, Y., and Russell, A. G.: Using High-
1018 Temporal-Resolution Ambient Data to Investigate Gas-Particle Partitioning of Ammonium over Different
1019 Seasons, *Environ. Sci. Technol.*, 54, 9834-9843, 10.1021/acs.est.9b07302, 2020.

1020 Zheng, B., Zhang, Q., Zhang, Y., He, K., Wang, K., Zheng, G., Duan, F., Ma, Y., and Kimoto, T.: Heterogeneous
1021 chemistry: a mechanism missing in current models to explain secondary inorganic aerosol formation during
1022 the January 2013 haze episode in North China, *Atmos. Chem. Phys.*, 15, 2031-2049, 2015a.

1023 Zheng, G. J., Duan, F. K., Su, H., Ma, Y. L., Cheng, Y., Zheng, B., Zhang, Q., Huang, T., Kimoto, T., Chang, D.,
1024 Pöschl, U., Cheng, Y. F., and He, K. B.: Exploring the severe winter haze in Beijing: the impact of synoptic
1025 weather, regional transport and heterogeneous reactions, *Atmos. Chem. Phys.*, 15, 2969-2983, 2015b.

1026 Zhou, H., Lü, C., He, J., Gao, M., Zhao, B., Ren, L., Zhang, L., Fan, Q., Liu, T., He, Z., Dudagula, Zhou, B., Liu,
1027 H., and Zhang, Y.: Stoichiometry of water-soluble ions in PM_{2.5}: Application in source apportionment for a
1028 typical industrial city in semi-arid region, Northwest China, *Atmos. Res.*, 204, 149-160,
1029 <https://doi.org/10.1016/j.atmosres.2018.01.017>, 2018.

1030 Zhu, Y., Li, W., Lin, Q., Yuan, Q., Liu, L., Zhang, J., Zhang, Y., Shao, L., Niu, H., Yang, S., and Shi, Z.: Iron

1031 solubility in fine particles associated with secondary acidic aerosols in east China, Environ. Pollut., 264,
1032 114769, <https://doi.org/10.1016/j.envpol.2020.114769>, 2020.

1033